Evidence for the Renormalization of the Mott Gap by Spin Correlations in Van der Waals Mott insulator $RuBr_3$

Kun Peng(彭坤)[1†], Bowen Zhang(张博文)[2†], Wei Yue(岳伟)[1], Lei Feng(冯磊)[3,6], Junliang Li(李军亮)[1], Runze Yu(于润泽)[2*], Xiaohu Zheng(郑晓虎)[3,5*], and Rui-Rui Du(杜瑞瑞)[1,4*]

[1]*International Center for Quantum Materials, School of Physics, Peking University, Beijing 100871, China*
[2]*Center for High-Pressure Science and Technology Advanced Research, Beijing 100093, China*
[3]*Beijing Academy of Quantum Information Sciences, Beijing 100193, China*
[4]*Hefei National Laboratory, Hefei 230088, China*
[5]*State Key Laboratory of Materials for Integrated Circuits, Shanghai Institute of Microsystem and Information Technology, Chinese Academy of Sciences, Shanghai 200050, China*
[6]*Corrosion and Protection Center, Institute for Advanced Materials and Technology, University of Science and Technology Beijing, Beijing 100083, China*

(Received 10 October 2025; accepted manuscript online 16 December 2025)

The interplay between spin and charge degrees of freedom in Mott insulators remains a central topic in strongly correlated electron systems. Using variable-temperature scanning tunneling microscopy/spectroscopy, we investigate the Van der Waals magnet $RuBr_3$, a candidate Kitaev quantum spin liquid material. At low temperatures, $RuBr_3$ exhibits a large correlated Mott gap exceeding 3 eV. As temperature increases, the gap softens significantly, decreasing to ∼0.7 eV by 200 K. This evolution coincides with magnetic phase transitions: a sharp reduction occurs near the Néel temperature ($T_N \approx 34$ K) upon loss of long-range antiferromagnetic order, followed by a gradual decline through the Kitaev paramagnetic regime. Comparison with α-$RuCl_3$ reveals that the dominant spin correlations—whether long-range order or short-range Kitaev interactions—govern the Mott gap renormalization. Our results highlight the essential role of spin-charge coupling in Mott physics and provide key insights into the electronic behavior of Kitaev materials across different magnetic phases.

DOI: 10.1088/0256-307X/43/2/020702 CSTR: 32039.14.0256-307X.43.2.020702

Mott insulators constitute a fascinating subject in the study of strongly correlated electron systems and are widely regarded as the parent compounds for various emergent quantum phenomena,[1–5] including quantum spin liquids (QSLs), high-temperature superconductivity, and quantum magnetism. In Mott and Hubbard's original theoretical framework, the insulating state was attributed solely to strong on-site Coulomb repulsion in half-filled electronic bands, without explicit consideration of the spin degrees of freedom.[6–9] Nevertheless, spin correlations within this gap can still give rise to a rich spectrum of charge-neutral excitations, such as (topological) magnons[10–12] and fractional spinons.[13,14] Recent theoretical advances posit that magnetic phases—including long-range order, frustration, and paramagnetism—can fundamentally govern charge dynamics in Mott insulators.[15–21] This influence manifests as a renormalization of the Hubbard bands,[22,23] which in turn can drive unconventional Mott transitions.[24–28] These insights have substantially enriched the landscape of Mott physics. Moreover, the intricate interplay between charge and spin degrees of freedom within the Mott–Hubbard framework is now considered essential for elucidating many long-standing puzzles in strongly correlated systems, such as the mechanism behind high-temperature superconductivity and the origin of various novel quantum excitations.[29–32] Monitoring the evolution of electronic states across magnetic transitions thus provides a critical means to probe spin–charge correlations and test theoretical predictions.

However, direct experimental verification has remained limited to date, largely due to the scarcity of ideal materials that simultaneously possess a relatively low magnetic phase transition temperature and easily measurable Mott–Hubbard bands. Van der Waals Kitaev QSL materials have emerged as a unique platform for investigating both non-Abelian anyon excitations[33,34] and Mott physics across a range of spin phases. Studies of leading candidates like α-$RuCl_3$ are revealing these Mott phenomena in phases ranging from long-range order and frustration to conventional paramagnetism.[35] In our recent study on α-$RuCl_3$, a leading Kitaev QSL candidate, we observed a pronounced softening of the Mott gap with increasing temperature, accompanied by the loss of spin fractionalization across the transition from a Kitaev paramagnetic (KPM) state to a conventional paramagnetic (CPM)

†These authors contributed equally to this work.
*Corresponding authors. Email: zhengxh@baqis.ac.cn; runze.yu@hpstar.ac.cn; rrd@pku.edu.cn
© 2026 Chinese Physical Society and IOP Publishing Ltd. All rights, including for text and data mining, AI training, and similar technologies, are reserved.

state.[36]

Here, we employ variable-temperature scanning tunneling microscopy/spectroscopy (STM/STS) to study $RuBr_3$, another Van der Waals Kitaev QSL candidate. Our STS measurements collected below T_N reveal that $RuBr_3$ is a strong Mott insulator, characterized by a correlated full gap exceeding 3 eV. As temperature increases, the full charge gap rapidly decreases to less than half near 30 K, consistent with the crossover to a KPM state. It is then followed by a smooth, continuous reduction, with the band gap reaching approximately 0.7 eV at 200 K. No further abrupt softening of the gap is observed when the temperature is raised to the crossover from the Kitaev quantum paramagnet to a conventional paramagnet (which we denote as T_K). Notably, the temperature evolution of the energy gap aligns closely with the deviation of the magnetic susceptibility from the Curie–Weiss fit. By comparing these results with those from α-$RuCl_3$, we further propose that long-range spin correlations—whether arising from long-range antiferromagnetic (AFM) order or short-range Kitaev interactions—play a significant role in renormalizing the Mott gap. Our findings not only provide key insights into the charge behavior of Kitaev QSL candidate materials across temperature regimes, but also call for a re-examination of Mott physics in this family of materials in light of the intricate coupling between charge and spin degrees of freedom.

In this study, single crystals of $RuBr_3$ were synthesized using a high-pressure cubic anvil apparatus, following a previously reported method.[37] Thin flakes were mechanically exfoliated from these high-quality bulk crystals in an argon-filled glovebox. To ensure reliable electron tunneling, the exfoliated flakes were transferred onto a freshly cleaved highly oriented pyrolytic graphite substrate using thermal release tape. Prior to measurements, the samples were degassed in an ultrahigh-vacuum (UHV) chamber (base pressure $\sim 8 \times 10^{-10}$ mbar) at 180 ℃ for 2 hours. All STM/STS measurements were subsequently performed in a commercial CAS Acme cryogen-free low-temperature SPM system. The STS spectra were acquired using a lock-in amplifier with a modulation frequency of 707 Hz and an amplitude of 10 mV.

The RuX_3 family (where X is a halogen: Cl, Br, I) constitutes a class of layered Mott insulators that serve as a key platform for investigating fundamental quantum magnetism and emergent topological phenomena. Among them, α-$RuCl_3$ stands out as the most prominent and widely studied member, exhibiting the most evident signatures of the predicted QSL behavior.[35,38–42] Crystallizing in an edge-sharing octahedral layered structure, these materials form two-dimensional honeycomb networks [Fig. 1(a)], which stack via weak Van der Waals interactions.[43] This layered nature facilitates mechanical exfoliation down to atomically thin flakes. Electronically, the Ru $4d^5$ orbitals adopt a low-spin state with total spin $S = 1/2$ and an effective orbital moment $l_{\text{eff}} = 1$ under crystal field splitting. Subsequent spin–orbit coupling (SOC) lifts the degeneracy, yielding a $j_{\text{eff}} = 1/2$ ground state separated from a $j_{\text{eff}} = 3/2$ manifold. Strong electron correlations further drive the system into a Mott insulating phase,[34] as depicted schematically in Fig. 1(b). This electronic and spin configuration favors the Kitaev interaction, rendering the RuX_3 family promising candidates for realizing the Kitaev QSL state. Notably, the distinct properties observed among $RuCl_3$, $RuBr_3$, and RuI_3 arise from the systematic variation in the balance among the three key magnetic interactions—Heisenberg (J), Kitaev (K), and symmetric off-diagonal (Γ) exchanges—as the halogen ion is changed, thereby modulating the electronic structure and magnetic couplings.

In this work, we study the electronic properties of $RuBr_3$ through comprehensive STM/STS measurements. This material crystallizes in the space group $R\bar{3}$ and features an ideal honeycomb lattice of Ru^{3+} ions [as shown in Fig. 1(a)], which remains structurally invariant across its magnetic transition.[44–47] This behavior contrasts with α-$RuCl_3$, which undergoes a structural transition from the high-temperature $C2/m$ phase to the low-temperature $R\bar{3}$ phase[48–52]—a change that may also affect charge dynamics within the Mott–Hubbard bands. Below a notably high Néel temperature of 34 K, $RuBr_3$ develops a zigzag AFM order, while it exhibits a significantly weaker Kitaev spin interaction between approximately 34 K and 160 K.[43,46,47,53,54] To minimize substrate effects and access the material's intrinsic properties, we selected thick $RuBr_3$ flakes (thickness >5 nm). Figure 1(c) presents an STM topographic image of the transferred sample, displaying clear atomic steps, confirming its layered Van der Waals nature. The corresponding height profile in Fig. 1(d) reveals a step height of ∼800 pm, consistent with the expected thickness of a $RuBr_3$ monolayer. Atomically resolved STM performed at 6 K on a flat terrace [Fig. 1(e)] resolves a honeycomb lattice formed by Ru atoms, with a measured lattice constant of approximately 6.2 Å. This value is slightly larger than that of α-$RuCl_3$ (5.96 Å), in agreement with previous reports,[21,25] which may account for the weak Kitaev spin coupling. The inset fast Fourier transform (FFT) pattern shows hexagonal Bragg reflection spots from both Ru and halogen sublattices, indicating negligible lattice strain.

The averaged dI/dV spectra acquired at 6 K exhibit a characteristic Mott-like lineshape, featuring a full correlation gap of approximately 3.3 eV alongside well-resolved upper and lower Hubbard bands (U&LHBs), as shown in Fig. 1(f). This experimentally determined gap is considerably larger than the values predicted by theoretical calculations[43,44] and those inferred from transport measurements,[37,47] in which the expected Mott gap is typically below 1 eV. To our knowledge, this work reports for the first time such a large Mott gap in $RuBr_3$—a finding that notably deviates from existing theoretical predictions.[44] This discrepancy calls into question the current understanding of the Mott gap in $RuBr_3$ and underscores the necessity of reexamining key electronic parameters, including the crystal field strength ($10Dq$) and the electron correlation energy (U), as well as the applicability of the conventional Mott–Hubbard model itself.

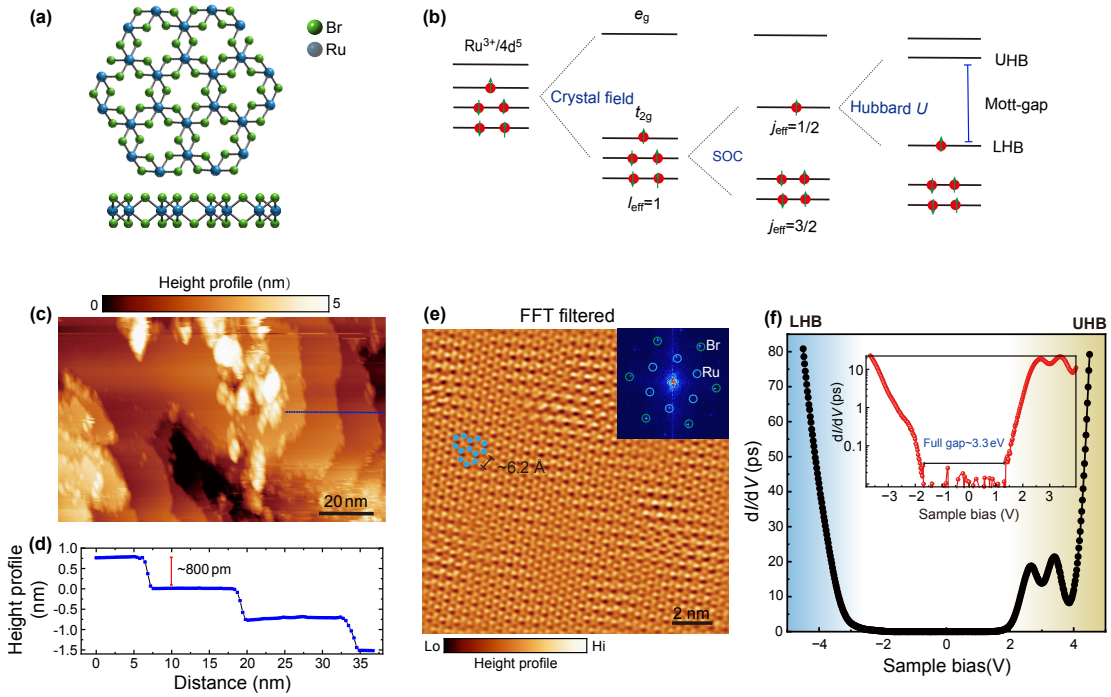

Fig. 1. The STM morphology and lattice structure of bulk $RuBr_3$. (a) Top and side views of the crystal structure of $RuBr_3$, which shares the same lattice configuration as other members of the RuX_3 family (where X represents a halogen: Cl, Br, or I). (b) A schematic diagram illustrates that the $4d^5$ orbitals of Ru atoms form a $j_{\rm eff} = 1/2$ Mott insulator characterized by Kitaev spin interactions, driven by the combined effects of crystal field splitting, strong SOC, and electronic correlations. (c) Large-view STM image of the transferred $RuBr_3$ ($V_{\rm bias} = 3.1\,{\rm V}$, $I_{\rm set} = 100\,{\rm pA}$). (d) Height profile along the blue dashed line in (c) illustrates the thickness of the $RuBr_3$ step. (e) Atomically resolved STM image of bulk $RuBr_3$ acquired at 6 K ($V_{\rm bias} = 1\,{\rm V}$, $I_{\rm set} = 400\,{\rm pA}$). The inset displays the FFT of (e), where the two sets of diffraction spots—colored green and blue—correspond to Br and Ru atomic lattices, respectively. (f) The average dI/dV spectrum of bulk $RuBr_3$ measured at 6 K ($V_{\rm bias} = 3\,{\rm V}$, $I_{\rm set} = 450\,{\rm pA}$), with the inset displayed on a logarithmic scale.

A similar inconsistency between computed and experimentally observed Mott gaps has been documented in α-$RuCl_3$, where significant variations also appear across different computational methods, experimental techniques, and temperatures. This phenomenon was recently interpreted as resulting from a spin-correlation-induced renormalization of the Mott gap during temperature change.[36]

To gain deeper insight into the electronic states and Mott characteristics of $RuBr_3$, we performed spatially resolved STS measurements under varied conditions. First, dI/dV spectra were acquired along a path crossing a typical surface vacancy defect, as indicated by the dashed line in the inset of Fig. 2(a). The resulting spectra reveal that the defect introduces in-gap states, characterized by pronounced peaks above the LHB, along with a slight shift in the UHB edge [red curves in Figs. 2(b) and 2(c)]. These features imply that defects in $RuBr_3$ can effectively renormalize the Mott gap. Second, we compared dI/dV spectra acquired across different terrace steps, as illustrated in the inset of Fig. 2(c). The negligible variation in spectral features indicates that the Mott electronic structure is largely independent of layer thickness. Finally, to access potential artifacts arising from the spread resistance effect,[55] we systematically varied the tip–surface distance while maintaining a fixed setpoint current ($I_{\rm set} = 450\,{\rm pA}$) and reducing the bias voltages (4.5 V, 3.5 V, and 2.5 V) during dI/dV acquisition. As shown in Figs. 2(d) and 2(e), the apparent total charge gap slightly decreases as the tip approaches the surface. Since both defects and spreading resistance are found to affect STS measurements in bulk $RuBr_3$, these factors must be carefully considered when probing the intrinsic Mott state. Therefore, to reliably track the temperature-dependent spectral evolution in subsequent experiments, we selected defect-free regions and maintained a constant tip–sample distance ($V_{\rm bias} = 3\,{\rm V}$, $I_{\rm set} = 450\,{\rm pA}$) throughout all measurements.

We measured the temperature-dependent electronic structure of $RuBr_3$ by acquiring dI/dV spectra from 6 K to 200 K—a range that spans its successive magnetic transitions: from an AFM state below the Néel temperature $T_{\rm N} = 34\,{\rm K}$ to a KPM phase, and further to a CPM state near $T_{\rm K} \approx 160\,{\rm K}$.[46] As illustrated in Fig. 3, the Mott gap exhibits strong temperature dependence, decreasing from 3.3 eV at the base temperature to 0.7 eV upon warming. This pronounced reduction cannot be attributed solely to thermal broadening of the Hubbard bandwidth. Notably, the reduced gap value at 200 K (~0.7 eV) aligns with the activation energy gap derived from transport measurements in the same temperature regime—on the order of several hundred millivolts.[37,47] Figure 3(b) plots the temperature-dependent dI/dV spectra on a logarithmic scale, highlighting a sharp drop near 30 K, close to the critical temperature $T_{\rm N}$. The absence of a temperature-induced structural phase transition in $RuBr_3$[46] rules out a lattice-driven origin for this gap reduction. Instead, the onset of gap reduction coincides with the crossover from

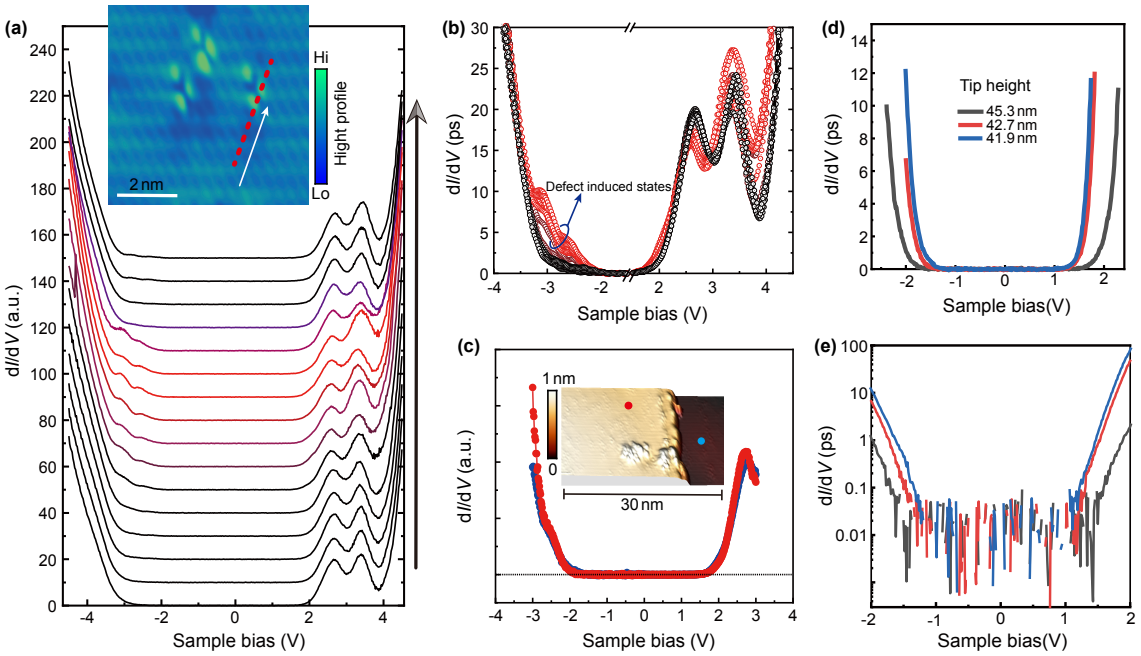

Fig. 2. STS measurements under various conditions. (a) dI/dV spectra collected along the red dashed line crossing the defect, as shown in the STM image of the inset ($V_{\rm bias} = 3\,{\rm V}$, $I_{\rm set} = 450\,{\rm pA}$). The red curves are spectra around the vacancy, while the black ones show the spectra far from the vacancy. (b) Direct comparison of the dI/dV spectra measured at the defect site and at locations far from the defect. (c) dI/dV spectra collected at the red and blue dots on adjacent steps, as indicated in the STM image, show layer-independent behavior ($V_{\rm bias} = 3\,{\rm V}$, $I_{\rm set} = 450\,{\rm pA}$). (d) Spread resistance during the dI/dV measurements with variation of tip–surface distances by changing the bias voltage at a fixed $I_{\rm set} = 450\,{\rm pA}$. (e) Logarithmic plots of the spectra in (d) present the magnitude of the full gap.

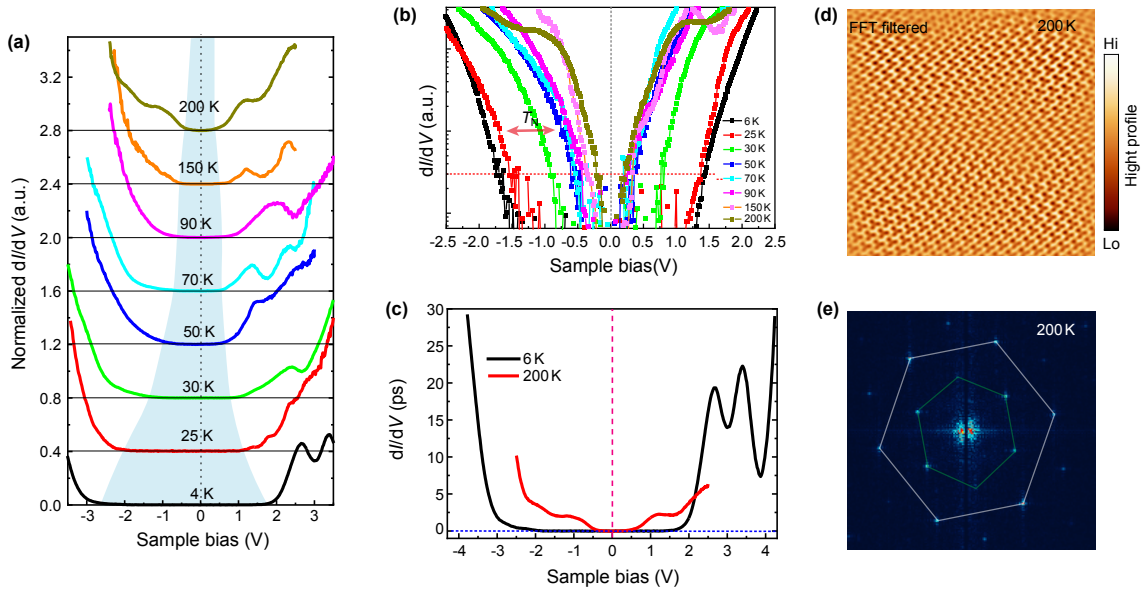

Fig. 3. Temperature-dependent dI/dV spectra on $RuBr_3$. (a) Averaged dI/dV spectra acquired at various temperatures ranging from 6 K to 200 K ($V_{\rm bias} = 3\,{\rm V}$, $I_{\rm set} = 450\,{\rm pA}$); the blue region indicates the magnitude of the correlation full gap. (b) Logarithmic plots of the spectra in (a) present the variation of the magnitude of the full gap. (c) A direct comparison of the dI/dV spectra acquired at 6 K and 200 K reveals a temperature-induced renormalization of the Mott gap. (d) FFT-filtered atomically resolved STM image on the $RuBr_3$ surface acquired at 200 K with $V_{\rm bias} = 2\,{\rm V}$, $I_{\rm set} = 450\,{\rm pA}$. (e) The FFT pattern of (d) exhibits a honeycomb arrangement of Bragg spots, preserving the original symmetry.

the AFM state to the KPM state, indicating a close coupling between the Mott charge state and the magnetism. With further increasing temperature, the full charge gap continues to decrease gradually, further implying a direct relationship between the Mott gap and the evolution of spin correlations. A direct comparison of the averaged dI/dV spectra taken at 6 K and 200 K, as shown in Fig. 3(c), confirms a substantial renormalization of the

Mott–Hubbard electronic structure, characterized by a prominent redistribution of spectral weight from the Hubbard bands toward the original Mott gap region. Moreover, atomically resolved STM images collected at 200 K, along with the preserved symmetry in the corresponding FFT patterns [Figs. 3(d) and 3(e)], rule out any significant lattice reconstructions over the temperature range studied. Collectively, these findings demonstrate that magnetic transitions, rather than lattice effects or thermal fluctuations, play a critical role in governing the renormalization of the Mott–Hubbard states in $RuBr_3$.

Experimental studies on both $RuBr_3$ and α-$RuCl_3$ have revealed a strong coupling between spin correlations and the Mott gap, though the two systems exhibit distinct behaviors. In α-$RuCl_3$, the crossover from the Kitaev paramagnet with short-range Ising spin correlations to the conventional paramagnet plays the dominant role in driving charge gap softening, with no significant change in the Mott gap observed across the AFM–KPM crossover.[36] In contrast, $RuBr_3$ exhibits a pronounced suppression of the Mott gap upon the loss of long-range AFM order, while no further sharp gap softening occurs during the KPM–CPM crossover. For a direct comparison, figure 4(a) presents the magnetic susceptibility of both compounds together with their Curie–Weiss fits (data from Refs. [35,37]). Upon cooling to approximately 100 K, the susceptibility curves of both materials progressively deviate from their Curie–Weiss fits; this deviation typically indicates the onset of spin correlations, though the specific type of correlation requires further analysis. In principle, it may arise from Kitaev spin correlations or other non-Heisenberg interactions. However, theoretical and experimental studies on the RuX_3 family (particularly α-$RuCl_3$) consistently show that anomalous phenomena (such as spin fractionalization and Majorana fermions) occurring below T_K (the onset temperature of the KPM state) are directly associated with Kitaev spin correlations.[56–59] Thus, in this family, the "deviation around 100 K" is often linked to the onset of Kitaev physics. It should be noted that the role of other non-Heisenberg interactions in Kitaev physics remains an open question and warrants further investigation.

This deviation, however, is less pronounced in $RuBr_3$. Moreover, $RuBr_3$ undergoes a broader AFM transition. These features collectively suggest that $RuBr_3$ possesses significantly weaker Kitaev interactions but stronger Heisenberg terms compared to α-$RuCl_3$, placing it further from the ideal Kitaev phase.[43,46] The residuals from the Curie–Weiss fits, shown in the inset of Fig. 4(b), further highlight this contrast: α-$RuCl_3$ shows a rapid increase beginning within the KPM regime, while $RuBr_3$ displays a similar rise starting already in the AFM phase. This implies that AFM Heisenberg interaction dominates the spin correlations in $RuBr_3$, whereas Kitaev interaction prevails in α-$RuCl_3$. Notably, the onsets of magnetism—AFM for $RuBr_3$ and KPM for α-$RuCl_3$—governed by the dominant spin correlations, align closely with the temperature ranges over which Mott gap renormalization occurs in both materials (around T_N for $RuBr_3$ and around T_K for α-$RuCl_3$), as depicted in Fig. 4(b). However, while long-range spin correlations prevail in the AFM state of $RuBr_3$ and the KPM state of α-$RuCl_3$, they may be absent in the KPM state of $RuBr_3$ due to its weak Kitaev interaction. We also note that a recent study on CrSBr, another two-dimensional Van der Waals magnet with Mott–Hubbard bands originating from Cr t_{2g} orbitals and dominant AFM spin correlations, reported similar renormalization of the Mott bands across the AFM-to-paramagnetic transition.[60] This parallel leads us to propose that the insulating state in a broad class of Mott insulators arises from the collective interplay of electron and spin correlations; the long-range spin correlations may play a critical role, regardless of whether the magnetism is AFM (e.g., Heisenberg-type) or KPM (e.g., Kitaev-type).

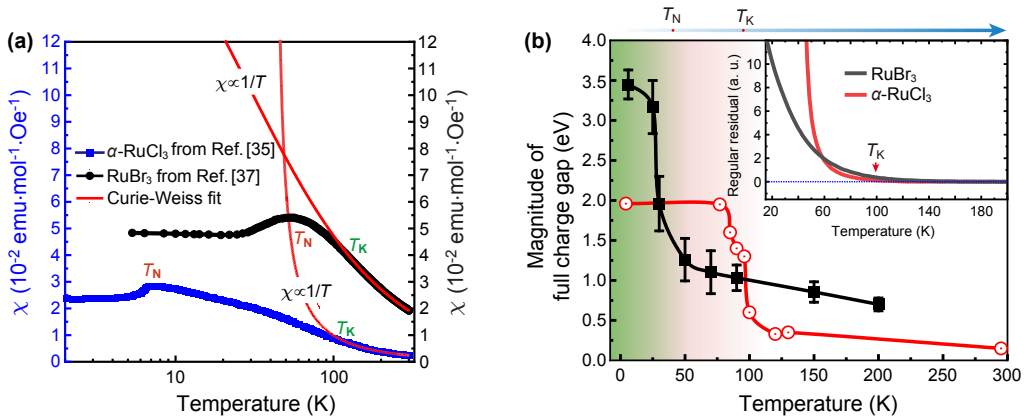

Fig. 4. The correlation between magnetic susceptibility and the Mott gap in both $RuBr_3$ and α-$RuCl_3$. (a) Plots of the magnetic susceptibility for $RuBr_3$ (black curve) and α-$RuCl_3$ (blue curve); the red curves represent Curie–Weiss fits. The deviation of the magnetic susceptibility from Curie–Weiss behavior indicates the emergence of spin correlations. T_K and T_N denote the critical temperatures associated with the emergence of the Kitaev QSL phase and the AFM ordering phase, respectively. (b) Comparison of the temperature-dependent variation in the full charge gap magnitude between $RuBr_3$ (black curve) and α-$RuCl_3$ (red curve). The $RuBr_3$ data points are extracted from Fig. 3(a), and the inset displays the residuals from the Curie–Weiss fitting. The sudden change in the energy gap is significantly correlated with the sudden change in the residuals.

In conclusion, our variable-temperature STM/STS study of the Van der Waals Mott insulator $RuBr_3$ directly demonstrates a profound temperature-induced renormalization of the Mott gap, which softens from over 3 eV at 6 K to approximately 0.7 eV at 200 K. This evolution is intimately tied to the material's magnetic transitions: a sharp reduction coincides with the loss of long-range AFM order at $T_N \sim 34$ K, followed by a gradual decline that tracks the decay of short-range Kitaev correlations. The contrasting behavior observed in α-$RuCl_3$ underscores how the nature of the dominant spin correlations—long-range order versus short-range Kitaev interactions—dictates the specific temperature dependence of the gap softening. Our findings establish that the insulating state in $RuBr_3$ arises from the collective interplay between charge and spin degrees of freedom and suggest that long-range spin correlations may play an important role in the framework of Mott–Hubbard insulating state, necessitating a revision of the conventional, purely charge-centric, static view of Mott physics. We expect this insight to motivate further theoretical and experimental efforts to enrich Mott physics and achieve targeted manipulation of correlated electronic states via their magnetic environment.

Acknowledgements. This work was supported by the National Natural Science Foundation of China (Grant Nos. 12474002 and 22171283 for R. Y.), the National Key Research and Development Program of China (Grant Nos. 2024YFA1409002 for R. R. D. and 2023YFA1406000 for R. Y.), the Quantum Science and Technology–National Science and Technology Major Project (Grant No. 2021ZD0302600 for R. R. D.), the Open Research Fund of State Key Laboratory of Materials for Integrated Circuits (Grant No. SKLJC-K2025-05 for X. H. Z.), and the Innovation Program for Quantum Science and Technology (Grant No. 2023ZD0300500 for X. H. Z.).

References

[1] Lee P A, Nagaosa N, and Wen X G 2006 *Rev. Mod. Phys.* **78** 17
[2] Anderson P W 1987 *Science* **235** 1196
[3] Anderson P W 1973 *Mater. Res. Bull.* **8** 153
[4] Anderson P W, Baskaran G, Zou Z, and Hsu T 1987 *Phys. Rev. Lett.* **58** 2790
[5] Zhou Y, Kanoda K, and Ng T K 2017 *Rev. Mod. Phys.* **89** 025003
[6] Hubbard J 1963 *Proc. R. Soc. London A* **276** 238
[7] Mott N F 1949 *Proc. Phys. Soc. A* **62** 416
[8] Mott N F 1968 *Rev. Mod. Phys.* **40** 677
[9] Roy S B 2019 *Mott Insulators: Physics and Applications* (Bristol: IOP Publishing)
[10] Braicovich L, van den Brink J, Bisogni V, Moretti Sala M, Ament L J P, Brookes N B, De Luca G M, Salluzzo M, Schmitt T, Strocov V N, and Ghiringhelli G 2010 *Phys. Rev. Lett.* **104** 077002
[11] McClarty P A 2022 *Annu. Rev. Condens. Matter Phys.* **13** 171
[12] Chen L, Chung J H, Gao B, Chen T, Stone M B, Kolesnikov A I, Huang Q, and Dai P 2018 *Phys. Rev. X* **8** 041028
[13] Mourigal M, Enderle M, Klöpperpieper A, Caux J S, Stunault A, and Rønnow H M 2013 *Nat. Phys.* **9** 435
[14] Faddeev L D and Takhtajan L A 1981 *Phys. Lett. A* **85** 5
[15] Song Y F, Deng Y, and He Y Y 2025 *Phys. Rev. Lett.* **134** 016503
[16] Ohashi T, Momoi T, Tsunetsugu H, and Kawakami N 2008 *Phys. Rev. Lett.* **100** 076402
[17] Park H, Haule K, and Kotliar G 2008 *Phys. Rev. Lett.* **101** 186403
[18] Vučičević J, Terletska H, Tanasković D, and Dobrosavljević V 2013 *Phys. Rev. B* **88** 075143
[19] Walsh C, Sémon P, Poulin D, Sordi G, and Tremblay A-MS 2019 *Phys. Rev. Lett.* **122** 067203
[20] Downey P O, Gingras O, Fournier J, Hébert C D, Charlebois M, and Tremblay A M S 2023 *Phys. Rev. B* **107** 125159
[21] Walsh C, Sémon P, Poulin D, Sordi G, and Tremblay A-MS 2019 *Phys. Rev. B* **99** 075122
[22] Han X J, Chen C, Chen J, Xie H D, Huang R Z, Liao H J, Normand B, Meng Z Y, and Xiang T 2019 *Phys. Rev. B* **99** 245150
[23] Long Z, Wang J, and Yang Y 2022 *Phys. Rev. B* **106** 195128
[24] Senthil T 2008 *Phys. Rev. B* **78** 045109
[25] Prots Y, Rößler S, Rößler U K, Rosner H, Akselrud L, Schmidt M, Fitch A, and Schwarz U 2023 *Z. Anorg. Allg. Chem.* **649** e202300140
[26] Mishmash R V, González I, Melko R G, Motrunich O I, and Fisher M P A 2015 *Phys. Rev. B* **91** 235140
[27] Li T, Jiang S, Li L, Zhang Y, Kang K, Zhu J, Watanabe K, Taniguchi T, Chowdhury D, Fu L, Shan J, and Mak K F 2021 *Nature* **597** 350
[28] Sheng D N, Motrunich O I, and Fisher M P A 2009 *Phys. Rev. B* **79** 205112
[29] Long Z, Wang J, and Yang Y 2023 *Phys. Rev. B* **108** 155127
[30] Zhang F C and Rice T M 1988 *Phys. Rev. B* **37** 3759
[31] Jahin A, Zhang H, Halász G B, and Lin S Z 2025 *Phys. Rev. Lett.* **134** 126501
[32] Kurosaki Y, Shimizu Y, Miyagawa K, Kanoda K, and Saito G 2005 *Phys. Rev. Lett.* **95** 177001
[33] Kitaev A 2006 *Ann. Phys.* **321** 2
[34] Jackeli G and Khaliullin G 2009 *Phys. Rev. Lett.* **102** 017205
[35] Do S H, Park S Y, Yoshitake J, Nasu J, Motome Y, Kwon Y S, Adroja D T, Voneshen D J, Kim K, Jang T H, Park J H, Choi K Y, and Ji S 2017 *Nat. Phys.* **13** 1079
[36] Yue W, Zheng X, Yang C, Peng K, and Du R R 2025 *Phys. Rev. Res.* **7** 043138
[37] Zhang B, Li X, Yan L, Li W, Li N, Zhao J, Liu X, Yu S L, Hu Z, Yang W, and Yu R 2025 *Chin. Phys. Lett.* **42** 027503
[38] Banerjee A, Yan J, Knolle J, Bridges C A, Stone M B, Lumsden M D, Mandrus D G, Tennant D A, Moessner R, and Nagler S E 2017 *Science* **356** 1055
[39] Banerjee A, Bridges C A, Yan J Q, Aczel A A, Li L, Stone M B, Granroth G E, Lumsden M D, Yiu Y, Knolle J, Bhattacharjee S, Kovrizhin D L, Moessner R, Tennant D A, Mandrus D G, and Nagler S E 2016 *Nat. Mater.* **15** 734
[40] Bruin J A N, Claus R R, Matsumoto Y, Kurita N, Tanaka H, and Takagi H 2022 *Nat. Phys.* **18** 401
[41] Kasahara Y, Ohnishi T, Mizukami Y, Tanaka O, Ma S, Sugii K, Kurita N, Tanaka H, Nasu J, Motome Y, Shibauchi T, and Matsuda Y 2018 *Nature* **559** 227
[42] Matsuda Y, Shibauchi T, and Kee H Y 2025 *Rev. Mod. Phys.* **97** 045003
[43] Kaib D A S, Riedl K, Razpopov A, Li Y, Backes S, Mazin I I, and Valentí R 2022 *npj Quantum Mater.* **7** 75
[44] Ersan F, Vatansever E, Sarikurt S, Yüksel Y, Kadioglu Y, Ozaydin H D, Aktürk O Ü, Aküncı Ü, and Aktürk E 2019 *J. Magn. Magn. Mater.* **476** 111

[45] Salavati M, Alajlan N, and Rabczuk T 2019 *Physica E* **113** 79
[46] Choi Y, Lee J H, Lee S, Wulferding D, Fujihara H, Sato F, Imai Y, Ohgushi K, Seong M J, and Choi K Y 2022 *Phys. Rev. B* **106** 174430
[47] Imai Y, Nawa K, Shimizu Y, Yamada W, Fujihara H, Aoyama T, Takahashi R, Okuyama D, Ohashi T, Hagihala M, Torii S, Morikawa D, Terauchi M, Kawamata T, Kato M, Gotou H, Itoh M, Sato T J, and Ohgushi K 2022 *Phys. Rev. B* **105** L041112
[48] Kubota Y, Tanaka H, Ono T, Narumi Y, and Kindo K 2015 *Phys. Rev. B* **91** 094422
[49] Johnson R D, Williams S C, Haghighirad A A, Singleton J, Zapf V, Manuel P, Mazin I I, Li Y, Jeschke H O, Valentí R, and Coldea R 2015 *Phys. Rev. B* **92** 235119
[50] Kim H S and Kee H Y 2016 *Phys. Rev. B* **93** 155143
[51] Glamazda A, Lemmens P, Do S H, Kwon Y S, and Choi K Y 2017 *Phys. Rev. B* **95** 174429
[52] Lin D, Ran K, Zheng H, Xu J, Gao L, Wen J, Yu S L, Li J X, and Xi X 2020 *Phys. Rev. B* **101** 045419
[53] Pearce J S, Kaib D A S, Ma Z, Ni D, Cava R J, Valentí R, Coldea R, and Coldea A I 2024 *Phys. Rev. B* **110** 214404
[54] Weinhold T, Wang C, Seewald F, Grinenko V, Imai Y, Sato F, Ohgushi K, Klauss H H, and Sarkar R 2024 *Phys. Rev. B* **109** 014440
[55] Frick J R, Sridhar S, Khansari A, Comstock A H, Norman E, O'Donnell S, Maggard P A, Sun D, and Dougherty D B 2023 *Phys. Rev. B* **108** 245410
[56] Rousochatzakis I, Kourtis S, Knolle J, Moessner R, and Perkins N B 2019 *Phys. Rev. B* **100** 045117
[57] Yoshitake J, Nasu J, and Motome Y 2017 *Phys. Rev. B* **96** 064433
[58] Yoshitake J, Nasu J, and Motome Y 2016 *Phys. Rev. Lett.* **117** 157203
[59] Yoshitake J, Nasu J, Kato Y, and Motome Y 2017 *Phys. Rev. B* **96** 024438
[60] Wu F, Zhang X F, Chen Y, Pei D, Zhan M W, Tao Z C, Chen C, Lu S P, Chen J Z, Tang S J, Wang X, Guo Y F, Yang L X, Zhang Y, Chen Y L, Mi Q X, Li G, and Liu Z K 2025 *Sci. China Phys. Mech. Astron.* **68** 267411